Adaptive Modulation and Coding With LDPC Codes and Retransmission for Ultraviolet Communication

Fei Long, Jingyin Tang, Lingfeng Li, Jingyang Chen, Chen Gong, *Senior Member, IEEE*, and Zhengyuan Xu, *Senior Member, IEEE*

***Abstract*—To adapt to different transmission power and distances, we design a rate-compatible transmission protocol to realize different transmission rates for ultraviolet (UV) communication. We have designed ensembles based on low-density parity-check (LDPC) codes, incorporating various code lengths and rates working under different channel conditions. Furthermore, the direct sequence spreading technique is adopted to obtain different channel codes working in weaker channel conditions. Through simulating the frame error rate (FER) performance across various signal and background radiation intensities, we obtain a table of switching thresholds for channel coding under distinct channel conditions. Different from that for radio-frequency (RF) communication with only one parameter of signal-to-noise ratio (SNR), the switching threshold table is constructed based on the combination of two parameters for UV Communication, the signal intensity and background radiation intensity. We also propose adaptive coding with hybrid automatic retransmission requests based on the combination of signal intensity and background intensity. It is verified through simulation that our designed system shows larger throughput under varying channel conditions compared with channel coding with a fixed rate in UV Communication.**

***Index Terms*—Wireless UV optical communication, adaptive modulation and coding, hybrid automatic retransmission request, low-density parity-check.**

I. Introduction

NON-LINE-OF-SIGHT (NLOS) scattering communication can serve as a viable contingency communication method, capable of achieving a certain transmission rate under intensive electromagnetic interference, while alleviating the stringent necessity for precise alignment between the transmitter and receiver [1], [2], [3]. Existing works on NLOS visible light communication (VLC) have been reported in [4], [5], [6]. Due to the significant interference posed by ambient light during daylight hours, ultraviolet (UV) communication within 200–280 nm spectrum [2] has emerged as a more favorable selection for optical wireless communication (OWC).

Manuscript received 24 January 2024; revised 19 March 2024; accepted 18 April 2024. Date of publication 23 April 2024; date of current version 6 May 2024. This work was supported by National Natural Science Foundation of China under Grant 62331024 and Grant 62171428. *(Corresponding author: Chen Gong.)*

The authors are with the CAS Key Laboratory of Wireless-Optical Communications, School of Information Science and Technology, University of Science and Technology of China, Hefei 230027, China (e-mail: ustclf@mail.ustc.edu.cn; tangjy27@mail.ustc.edu.cn; lilingfeng@mail.ustc.edu.cn; chenjingyang@mail.ustc.edu.cn; cgong821@ustc.edu.cn; xuzy@ustc.edu.cn).

Digital Object Identifier 10.1109/JPHOT.2024.3392669

UV communication can be effectively characterized using Poisson channels. Extensive research has been dedicated to investigating the capacity of both continuous-time and discrete-time channels, as [7], [8], [9], [10]. A static combining method is proposed in [11] to combine the outputs of the multiple photomultiplier tube (PMT) receivers. In terms of relay communications, work [12] proposes an alternate iterative-newton method (AINM) and a space-division coupled full-duplex relay configuration in multi-hop full-duplex relay links. Work [13] investigates the performance of a UAV-assisted, asymmetric and dual-hop radio frequency (RF)/free space optical (FSO) communication system with amplified-and-forward relay protocol. Work [14] studies the performance of mixed millimeter-wave RF and FSO communication system in a highly scalable and cost-effective solution for the fifth-generation (5G) mobile backhaul networks. In terms of channel attributes, the literature studies link gain models and pulse response models, as in [15]. Moreover, work [16] introduces a queue-based detection algorithm built on the maximum likelihood ratio, while [17], [18] propose signal detection techniques grounded in receiver diversity.

On the other hand, UV communication is significantly affected by atmospheric absorption and scattering. Adaptive modulation and coding (AMC) scheme can improve the communication efficiency and reliability, depending on the predicted channel state to determine the modulation and coding policy from the feasible candidates at the transmitter. It enables the adjustment of transmission modes based on the channel state information at the transmitting node [19]. Works [20], [21] have proposed a model for continuous-rate adaptive modulation and coding. Work [22] studies the performance of AMC technology in Rayleigh channels. Furthermore, work [23] introduces an adaptive modulation and coding model tailored for free-space optical links. In terms of optical communications, work [24] proposes a reinforcement learning-based AMC scheme for underwater communication. Work [25] proposes a novel adaptive cooperation (AC) protocol for FSO communications and extends the AC protocol to AMC, which improves the system throughput. AMC can be adopted for UV communication. Therefore, we introduce AMC to UV communication to improve system throughput.

The contribution of this paper is to apply AMC and retransmission in UV communication. Different from that for RF communication based on only one parameter of signal-to-noise ratio (SNR), in this work, the AMC protocol is based on the combination of two parameters, signal and background intensities. In this work, we design a rate-compatible transmission protocol for

© 2024 The Authors. This work is licensed under a Creative Commons Attribution 4.0 License. For more information, see https://creativecommons.org/licenses/by/4.0/

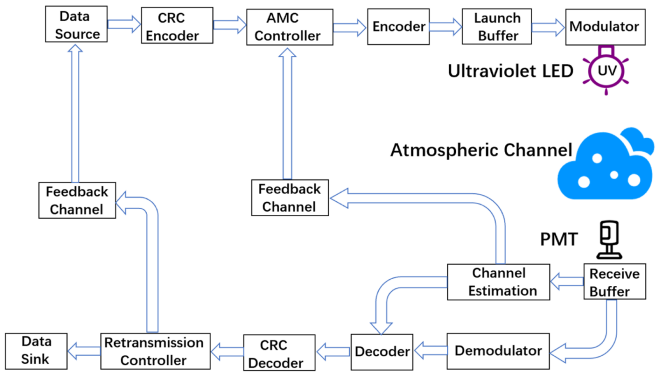

Fig. 1. The block diagram of NLOS UV scattering communication system with adaptive modulation and coding.

UV communication based on the combination of signal intensity and noise intensity of the channel. Specifically, we design a set of low-density parity-check (LDPC) codes with different rates for different channel conditions, and further adopt direct spreading for even weaker channel condition. Through simulation, we evaluate the performance of these codes under different signal and background intensities. The mode-switching threshold table is determined using a frame error rate (FER) prioritization criterion. We construct and implement an automatic retransmission request technique during data transmission. We simulate the time-latency of code groups and evaluate the latency for channel estimation and synchronization by two field-programmable gate array (FPGA) boards, respectively, constructing the forward link and the feedback link using the stop-and-wait protocol. Such feedback link allows the receiver to send transmission mode and retransmit information to the transmitter. Considering NLOS and line-of-sight (LOS) scenarios, we conduct experimental measurements and numerical simulations for channel parameters. Results in both scenarios demonstrate that our designed system shows larger throughput with single channel coding.

The remainder of this paper is organized as follows. Section II introduces the system model. Section III constructs a set of codes with different rates. Section IV proposes automatic retransmission request based transmission protocol. Section V shows the system throughput results based on the real channel measurement results. Finally, Section VI concludes this paper.

II. System Model

We consider an UV scattering communication system, as depicted in Fig. 1. Due to the scattering and absorption characteristics of the atmosphere, UV communication can achieve NLOS transmission. The optical signal emitted by the transmitter will show extremely weak discrete photon signals after scattering and absorption, resulting in photon-level signal. In addition, part of the sunlight will penetrate the atmosphere, causing ambient interference. Based on the detection bit error ratio (BER) and achievable rate formula for a photon-counting receiver, the atmospheric channel of UV communication needs to be characterized by the combination of signal intensity and noise intensity. The received signal intensity varies with different transmission power levels and distances, resulting in varying achievable transmission rates. However, the AMC for RF and FSO communication depends on SNR, rather than the combination of signal intensity and noise intensity. Therefore, it becomes imperative to develop a transmission mechanism adapting to diverse levels of received signal and noise intensities.

At the transmitter side, we select an appropriate transmission mode and determine whether data frame retransmission is necessary based on feedback from the receiver side. The sending system adds a CRC check code to the source output information and then performs channel coding. The channel-encoded signal is put into a buffer and then transmitted using an UV LED light. At the receiver side, a PMT is employed to capture the optical signal. The receiver compares the channel state information and coding mode-switching table to select an appropriate transmission mode. The receiver adopts stop-and-wait protocol to feedback the transmission mode and retransmission of information to the transmitter, which facilitates the transmission selection and data frame retransmission under varying channel conditions.

III. Modulation and Coding Selection

Based on the system block diagram depicted in Fig. 1, we characterize the coding and modulation sets adopted for designing adaptive modulation and coding.

A. On-Off Keying Modulation

On-Off Keying (OOK) is adopted to modulate the signal, where the UV LED on and off states represent the transmission of information bits one and zero, respectively. At the receiver, due to large path loss, the received signal exhibits discrete photon characteristics. When the transmitter sends "1" and "0", the number of received photons follows Poisson distribution [26], given by

$$P(N_i = n|s_i = 1) = \frac{(\lambda_s + \lambda_b)^n}{n!} e^{-(\lambda_s+\lambda_b)},$$
$$P(N_i = n|s_i = 0) = \frac{\lambda_b^n}{n!} e^{-\lambda_b}, \quad (1)$$

where λ_s and λ_b denote the average number of detected photoelectrons for the signal and background noise components. Under symbol rate R_s, the signal intensity is given by

$$\lambda_s = \frac{\eta g_t \tilde{P}_t}{h v R_s}, \quad (2)$$

where η, h, v, g_t and $\tilde{P}_t$ denote the receiver quantum efficiency, Planck's constant, the signal frequency, the path loss between the transmitter and receiver, and the signal transmission power, respectively.

B. Channel Coding Design

1) LDPC Code Construction: LDPC codes with different rates are adopted for different signal intensities. Moreover, spreading codes combined with low-rate LDPC codes are adopted for even weaker signal intensity.

Quasi-Cyclic Low-Density Parity-Check (QC-LDPC) codes are adopted. The parity-check matrix is determined by H_b and L, where H_b is an $m \times n$ base matrix and L represents the size of shift factor. The parity-check matrix of QC-LDPC codes can be represented as follows

$$H = \begin{bmatrix} {H_b}^{p_{11}} & {H_b}^{p_{12}} & \cdots & {H_b}^{p_{1n}} \\ {H_b}^{p_{21}} & {H_b}^{p_{22}} & \cdots & {H_b}^{p_{2n}} \\ \vdots & \vdots & \cdots & \vdots \\ {H_b}^{p_{m1}} & {H_b}^{p_{m2}} & \cdots & {H_b}^{p_{mn}} \end{bmatrix}_{mL \times nL}, \quad (3)$$

where p_{ij} represents the (i, j) element in H_b matrix, and ${H_b}^{p_{ij}}$ denotes a cyclic shift matrix or an all-zero matrix determined by p_{ij}. The parity-check matrix H can be decomposed into multiple identically sized cyclic shift matrices or all-zero matrices ${H_b}^{p_{ij}}$.

2) Channel Estimation and LLR Information Calculation: The synchronization sequence is also adopted for channel parameters estimation. Usually, the received signal is divided into M chips according to the duration for synchronization accuracy. Therefore, the numbers of pulses in a received signal are stored in an $1 \times M$ matrix $\mathbf{C_1}$. Let an $L \times M$ matrix $\mathbf{C_s}$ denote the number of pulses in the L-bit pilot symbols corresponding to synchronization sequence $\mathbf{s}$, where the number of pulses for each symbol can be obtained via merging those of consecutive M chips. Hence, the mean of signal intensity and noise intensity, denoted as λ_s and λ_b, respectively, can be estimated by following unbiased estimation [27]

$$\hat{\lambda}_s + \hat{\lambda_b} = \frac{\mathbf{s^T C_s 1_M}}{\mathbf{s^T 1_L}},$$
$$\hat{\lambda}_b = \frac{\bar{\mathbf{s}}^{\mathbf{T}} \mathbf{C_s 1_M}}{\bar{\mathbf{s}}^{\mathbf{T}} \mathbf{1_L}}, \quad (4)$$

where $\mathbf{1_M}$ and $\mathbf{1_L}$ are all-one M-dimensional and L-dimensional column vectors, respectively; $\mathbf{s}$ is the synchronization sequence, as an L-dimensional column vector; and $\bar{\mathbf{s}}$ represents $\mathbf{1_L} - \mathbf{s}$. According to (1), the log-likelihood ratio (LLR), denoted as $L(P_i)$, is given by

$$L(P_i) = \log \frac{P\{z_i = N | s_i = 1\}}{P\{z_i = N | s_i = 0\}} = \log \frac{\frac{(\hat{\lambda}_s + \hat{\lambda}_b)^N}{N!} e^{-(\hat{\lambda}_s + \hat{\lambda}_b)}}{\frac{\hat{\lambda}_b^N}{N!} e^{-\hat{\lambda}_b}}$$
$$= N \log \frac{\hat{\lambda}_s + \hat{\lambda}_b}{\hat{\lambda}_b} - \hat{\lambda}_s. \quad (5)$$

Here the direct spreading is performed to obtain a lower-rate code, such that the data can be transmitted in weaker channel states. To ensure communication efficiency, we choose a four-fold spreading sequence. For spread spectrum codes, we assume a four-fold spreading code sequence denoted as c_j^i $(i = 0, 1; j = 1, 2, 3, 4)$, where the values of c_j^i can be either 0 or 1. Specifically, when the transmitter sends the encoded bit 1, the code block sent by the transmitter is represented as $[c_1^1, c_2^1, c_3^1, c_4^1]$. When the transmitter sends the encoded bit 0, the code block sent by the transmitter is represented as $[c_1^0, c_2^0, c_3^0, c_4^0]$. Let the photon count value for c_j^i be N_j. Based on the estimation results, the probability is given according to the following Poisson distribution model

$$P(N_1, N_2, N_3, N_4 | s_t = i) = \prod_j^4 \frac{\hat{\lambda}_{ij}^{N_j}}{N_j!} e^{-\hat{\lambda}_{ij}},$$
$$\hat{\lambda}_{ij} = c_j^i \hat{\lambda}_s + \hat{\lambda}_b,$$
$$i = 0, 1,$$
$$j = 1, 2, 3, 4, \quad (6)$$

where N_j represents the number of photons received by the receiver when the transmitter sends c_j^i. The log-likelihood ratio information can be obtained as follows

$$L(P_t) = \log \left(\frac{P(N_1, N_2, N_3, N_4 | s_t = 1)}{P(N_1, N_2, N_3, N_4 | s_t = 0)} \right)$$
$$= \sum_{j=1}^4 N_j \log \left(\frac{c_j^1 \hat{\lambda}_s + \hat{\lambda}_b}{c_j^0 \hat{\lambda}_s + \hat{\lambda}_b} \right) + \hat{\lambda}_s \sum_{j=1}^4 \left(c_j^0 - c_j^1 \right). \quad (7)$$

TABLE I
ADAPTIVE MODULATION AND CODING CODE GROUP

Rate	Code Group	
0.192	(19968, 3840)	(13312, 2560)
0.324	(26112, 8448)	(17408, 5632)
0.588	(6528, 3840)	(4352, 2560)
0.815	(10368, 8448)	(6912, 5632)

Rate	Code Group		
0.192	(6656, 1280)	(3328, 640)	(1664, 320)
0.324	(8704, 2816)	(4352, 1408)	(2176, 704)
0.588	(2176, 1280)	(1088, 640)	(544, 320)
0.815	(3456, 2816)	(1728, 1408)	(864, 704)

C. Performance of LDPC Codes

We adopt the QC-LDPC code in 5G, as a type of structured LDPC code generated by the superposition construction method. The basis matrices with 0.192, 0.324, 0.588 and 0.815 code rates are employed. We construct 20 LDPC codes with different code rates and code lengths based on the scheme mentioned above, as shown in Table I. To make the channel coding usable in weaker channel environments, we have performed a 4-fold direct spreading process on the code sets of 0.192 code rate and 0.324 code rate. A 4-fold direct spreading is employed, which expands the encoded sequence of bits "1" and "0" into "1010" and "0101" symbols for transmission, respectively. It results in an effective system data rate that is reduced to one-quarter of the original data rate, allowing for improved performance in weaker power reception.

Thus, we obtained 20 QC-LDPC codes and 10 spreading codes combined with low-rate LDPC codes, totaling 30 sets of channel codes with different performances, as the modulation and coding scheme (MCS) scheme for the system.

TABLE II
THE THRESHOLDS FOR THE CODING SCHEME AT A TARGET FRAME ERROR RATE OF 10^{-2}

Code rate	0.192 spread spectrum code					0.324 spread spectrum code					0.192				
	Th_1	Th_2	Th_3	Th_4	Th_5	Th_6	Th_7	Th_8	Th_9	Th_{10}	Th_{11}	Th_{12}	Th_{13}	Th_{14}	Th_{15}
$\lambda_b = 0.1$	0.35	0.35	0.35	0.35	0.35	0.5	0.5	0.5	0.5	0.55	0.8	0.85	0.85	0.9	0.95
$\lambda_b = 0.2$	0.45	0.45	0.45	0.45	0.45	0.6	0.6	0.6	0.65	0.65	1	1	1.05	1.05	1.15
$\lambda_b = 0.3$	0.5	0.5	0.5	0.5	0.55	0.66	0.68	0.68	0.68	0.75	1.1	1.1	1.15	1.2	1.25
$\lambda_b = 0.4$	0.55	0.55	0.55	0.55	0.57	0.75	0.75	0.75	0.75	0.78	1.2	1.25	1.25	1.3	1.4
$\lambda_b = 0.5$	0.6	0.6	0.6	0.6	0.62	0.79	0.85	0.85	0.85	0.85	1.3	1.3	1.35	1.4	1.5
$\lambda_b = 0.6$	0.65	0.65	0.65	0.65	0.66	0.88	0.88	0.88	0.88	0.92	1.35	1.35	1.45	1.5	1.6
$\lambda_b = 0.7$	0.7	0.7	0.7	0.7	0.72	0.94	0.94	0.94	0.94	0.98	1.45	1.45	1.55	1.6	1.65
$\lambda_b = 0.8$	0.74	0.74	0.74	0.74	0.76	1	1	1	1	1.05	1.55	1.55	1.6	1.65	1.7
$\lambda_b = 0.9$	0.75	0.75	0.75	0.75	0.8	1.04	1.04	1.04	1.04	1.06	1.6	1.6	1.65	1.75	1.85
$\lambda_b = 1.0$	0.8	0.8	0.8	0.8	0.84	1.06	1.06	1.06	1.09	1.11	1.65	1.65	1.75	1.8	1.9

Code rate	0.324					0.588					0.815				
	Th_{16}	Th_{17}	Th_{18}	Th_{19}	Th_{20}	Th_{21}	Th_{22}	Th_{23}	Th_{24}	Th_{25}	Th_{26}	Th_{27}	Th_{28}	Th_{29}	Th_{30}
$\lambda_b = 0.1$	1.3	1.3	1.32	1.35	1.45	2.85	2.95	3.1	3.3	3.5	5.1	5.2	5.3	5.5	5.9
$\lambda_b = 0.2$	1.49	1.51	1.53	1.56	1.64	3.3	3.35	3.45	3.7	3.9	5.7	5.8	5.9	6.1	6.5
$\lambda_b = 0.3$	1.65	1.65	1.7	1.75	1.85	3.6	3.7	3.8	4	4.2	6	6.3	6.3	6.6	6.9
$\lambda_b = 0.4$	1.8	1.8	1.85	1.9	1.95	3.84	3.87	4	4.2	4.5	6.3	6.5	6.7	6.9	7.3
$\lambda_b = 0.5$	1.9	1.9	2	2.05	2.1	4.05	4.1	4.3	4.5	4.8	6.7	6.8	7	7.3	7.6
$\lambda_b = 0.6$	2.1	2.1	2.1	2.15	2.25	4.2	4.3	4.5	4.7	5	7	7.1	7.3	7.6	7.9
$\lambda_b = 0.7$	2.15	2.15	2.2	2.25	2.35	4.4	4.5	4.6	4.8	5.2	7.22	7.28	7.5	7.9	8.2
$\lambda_b = 0.8$	2.25	2.25	2.3	2.35	2.45	4.6	4.7	4.8	5	5.4	7.45	7.5	7.7	8.1	8.5
$\lambda_b = 0.9$	2.35	2.35	2.4	2.45	2.55	4.7	4.8	5	5.2	5.5	7.65	7.75	8	8.3	8.7
$\lambda_b = 1.0$	2.45	2.45	2.5	2.55	2.65	4.9	5	5.1	5.4	5.8	7.9	8	8.2	8.5	8.9

We specify the NLOS UV communication system under consideration. Let the transmission symbol rate of OOK modulation $R_b = 1$ Mbps and the number of chips in a symbol $M = 10$. Note that the solar background radiation is approximately 1×10^4 to 5×10^4 counts per second at wavelength 266 nm. Hence we adopt a certain margin for the background radiation intensity within each symbol duration and set $\lambda_b = \{0.1, 0.2, 0.3, 0.4, 0.5, 0.6, 0.7, 0.8, 0.9, 1.0\}$. Based on the FER simulation results, according to the threshold determination criteria, the transmission mode switching thresholds can be obtained as shown in Table II.

Based on the simulation results, it is evident that within encoding groups operating at the same code rate, as the code length increases, the required signal intensity (λ_s) decreases when reaching the target frame error rate. This indicates that longer codes require lower signal intensity for reliable transmission at the same frame error rate. However, as the code rate decreases to lower levels, the improvement in encoding performance due to increased code length becomes negligible. In such cases, certain encodings demonstrate a characteristic where the required signal intensity for achieving the desired error rate remains roughly equal.

Considering the higher decoding complexity and latency associated with longer codes, especially within encoding groups with similar switching thresholds, there is a preference for selecting encoding schemes with shorter code lengths. This preference stems from the fact that shorter code length schemes may maintain acceptable performance while reducing decoding complexity and latency. Therefore, when selecting encoding schemes in practical applications, factors such as signal intensity, code length, frame error rates, and decoding complexity should be taken into account to choose the most suitable encoding scheme for a specific scenario.

IV. HYBRID AUTOMATIC RETRANSMISSION REQUEST BASED TRANSMISSION PROTOCOL

In this section, we determine an MCS switching algorithm based on simulated FER results, incorporating a two-dimensional variable of signal intensity and noise intensity. Introducing hybrid automatic repeat request (HARQ) technology enhances system reliability. Simulations and experiments are adopted to assess encoding and decoding latencies for various codes, as well as end-to-end synchronization delays. Based on the results, we construct frame structures for both forward and feedback links, employing a stop-and-wait protocol for feedback transmission.

A. Channel Coding Switching

Unlike the SNR concept in RF communications, UV communication needs to determine the appropriate code rate based on two parameters, λ_s and λ_b, a two-dimensional characterization of channel conditions. Therefore, the receiver needs to estimate both signal intensity and noise intensity. Since the coding codebook is shared between the receiver and the transmitter, in order to reduce the amount of information of the feedback link, the receiver selects the appropriate coding scheme and feeds back the index to the transmitter.

The modulation and coding selection based on channel estimation becomes a pivotal factor, which involves setting

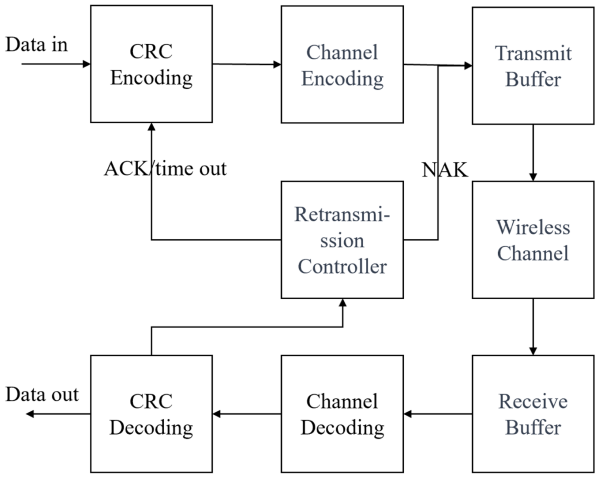

(a) HARQ system structural model diagram.

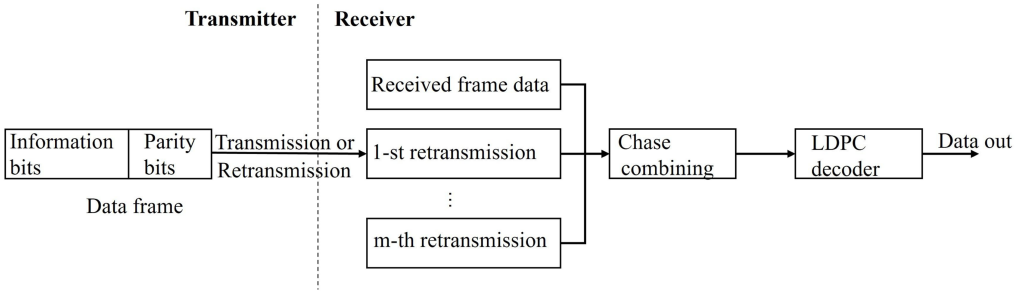

(b) The Chase combining retransmission process.

Fig. 2. HARQ protocol block diagram.

thresholds for switching transmission modes. The receiver matches the channel estimation information with these thresholds to determine the appropriate coding rate. In this work, we adopt FER as the criterion for transmission mode switch. As UV communication channels are characterized by two parameters, the determination of AMC switching threshold table requires an evaluation of both parameters to derive threshold values. This process is shown in the following steps. Firstly, we categorize the noise intensity into m quantization levels $\{\lambda_{b1}, \lambda_{b2}, \ldots, \lambda_{bm}\}$ and each quantization level λ_{bj} corresponds to a set of signal intensity thresholds $\{Th_{i1}, Th_{i2}, \ldots, Th_{in}\}$. Set $\lambda_{b0} = 0$. If the estimated noise intensity $\hat{\lambda}_b$ in set $(\lambda_{b_{i-1}}, \lambda_{b_i}]$, we consider the noise intensity of the channel to be at the i_{th} quantization level. We compare the estimated signal intensity $\hat{\lambda}_s$ with the signal intensity thresholds corresponding to λ_{bi}. If $\hat{\lambda}_s$ is within the set $[Th_{ij}, Th_{ij+1})$, then the transmission mode is selected to be the TM_{ij} corresponding to Th_{ij}. If $\hat{\lambda}_s$ is greater than λ_{bm} or $\hat{\lambda}_s$ is less than Th_{i1}, it is considered that the current channel conditions cannot be satisfied for reliable communication, where only the synchronization sequence is transmitted. The transmission scheme determination process can be described as follows in Algorithm 1.

B. Retransmission Request Types and Soft Information Fusion

Forward Error Correction (FEC) and HARQ techniques are commonly employed for error control. Within the error correction capability of FEC, errors are automatically corrected. Otherwise, the receiver requests the transmitter to retransmit the information, as depicted in Fig. 2(a).

Upon input of information, it undergoes cyclic redundancy check (CRC) verification. The data verified by CRC is then subjected to channel encoding. The data, once encoded, is directed to the transmit buffer for subsequent data retransmissions. At the receiver, upon receipt of information from the transmitter, the received data is initially stored in the receiving buffer, for merging and decoding with subsequent retransmitted data, which is then passed through a decoder. The decoded data undergoes CRC validation, and the CRC validator feeds back the validation information to the retransmission controller. If the retransmission controller detects an error in the CRC of the frame and the frame has not reached the preset maximum number of retransmissions, it will control the transmitter to retransmit the frame during the next transmission. Otherwise, it is considered that the frame does not need to undergo the retransmission process.

HARQ introduces a combining decoding mechanism that merges retransmitted system information with the information stored in the receive buffer for decoding. Presently, HARQ employs mainly two combining mechanisms: Chase combining [28] and Incremental Redundancy (IR) combining [29]. As puncturing and deletion are not adopted, IR combining is not adopted. Chase combining involves retransmitting the erroneous information frame during each retransmission, while the receiver

Algorithm 1 Transmission Mode Selection Algorithm

Input: Estimation of signal intensity $\hat{\lambda}_s$ and noise intensity $\hat{\lambda}_b$;
Output: Transmission mode MCS;
Set: Noise intensity set $\{\lambda_{b0}, \lambda_{b1}, \lambda_{b2}, \ldots, \lambda_{bm}\}$, signal intensity threshold set $\{Th_{i1}, Th_{i2}, \ldots, Th_{in}, +\infty\}$ under λ_{bi} and transmission mode TM_{ij} corresponding to threshold Th_{ij};

Initialize: $i \leftarrow 0$, $j \leftarrow 0$ and flag $\leftarrow 0$
if $\hat{\lambda}_b > \lambda_{bm}$ **Then**
    $MCS \leftarrow TM_0$
else
    while NOT flag do
        $i \leftarrow i + 1$
        if $\hat{\lambda}_b$ in set $(\lambda_{b_{i-1}}, \lambda_{b_i}]$ **Then**
            if $\hat{\lambda}_s < Th_{i1}$ **Then**
                $MCS \leftarrow TM_0$
                flag $\leftarrow 1$
            else
                while NOT flag do
                    $j \leftarrow j + 1$
                    if $\hat{\lambda}_s$ in set $[Th_{ij}, Th_{ij+1})$ **Then**
                        $MCS \leftarrow TM_{ij}$
                        flag $\leftarrow 1$
                    end if
                end while
            end if
        end if
    end while
end if
return MCS

The TM_0 in Algorithm 1 indicates the transmission mode of only transmitting synchronization sequences.

combines the retransmitted information using the maximal ratio combining principal, as depicted in Fig. 2(b).

Chase combining mechanism stores each retransmission information in the receiver's buffer. For every retransmission, weighted merging with the previously stored information is adopted. After M retransmissions, the receiver obtains the merged LLR as follows

$$L(P_i) = \sum_{l=1}^{M} L^l(P_i) w_l \, i = 1, 2, \ldots, N, \tag{8}$$

where $L^l(P_i)$ represents the prior information of the i^{th} codeword during the l^{th} retransmission, w_l indicates the confidence of the current codeword's initial prior information. Since larger ratio of signal intensity over noise intensity leads to more useful information contained in the received signal, the ratio of signal intensity to noise intensity is chosen to calculate the confidence factor. Therefore, w_l is given by

$$w_l = \frac{\gamma_l}{\sum_{k=1}^{M} \gamma_k}, \tag{9}$$

TABLE III
ENCODER AND DECODER LATENCY TESTING SIMULATION SYSTEM PARAMETERS

	Encoder	Decoder
Processing Clock	200 MHz	200 MHz
Input data bit width	8 bits	8 bits
Output data bit width	8 bits	8 bits

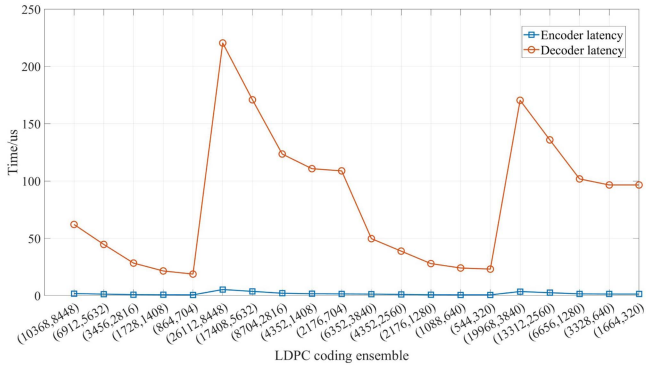

Fig. 3. Encoding and decoding latencies of different LDPC codes.

where γ_l and γ_k represent the ratios of signal intensity to noise intensity during the l^{th} and k^{th} transmission, respectively. By utilizing the ratio as a weight, the retransmitted LLR information can be weighted and combined, resulting in a certain diversity gain.

C. Communication Link Time Slot Division

Time-division multiplexing is adopted to construct the forward information link and the retransmission data link. Before designing the protocol, it is necessary to simulate the time-latency characteristics of different code groups, and collect the time latency. LDPC encoder/decoder IP core in Vivado is adopted to realize the LDPC coding and decoding and construct a real-time system simulation platform. The parameters of the simulation system are shown in Table III. The simulation results of encoding and decoding latency are shown in Fig. 3, where the longest encoding and decoding latencies are generated by the (26112, 8448) LDPC code. Specifically, the maximum encoding latency is 5.305 microseconds, and the maximum decoding latency is 220.515 microseconds. The encoding latency of different LDPC codes varies slightly. However, the decoding latency increases substantially in code length.

To evaluate the latency for channel estimation and synchronization, two FPGA boards are adopted as the transmitter and receiver as shown in Fig. 4. As shown in Fig. 5, among 50 groups, and the average synchronization delay is 258.9132 us. Since it is larger than the longest decoding delay, there is no timing conflict when different code groups are transmitted. To enhance data transmission reliability, we incorporate a guard interval between different data frames, which is significantly longer compared with the longest transmission distance. The resulting structure of the transmitted frame is shown in Fig. 6.

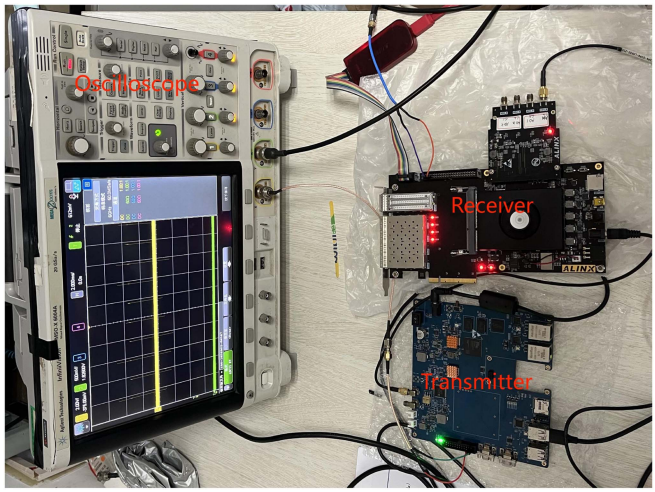

Fig. 4. End-to-End latency test hardware system.

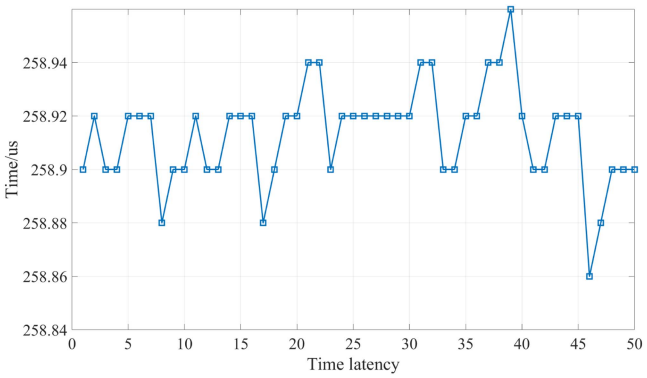

Fig. 5. 50 sets of end-to-end synchronized delay test results when the symbol rate is 1 Mbps and a 256-bit pilot sequence is used.

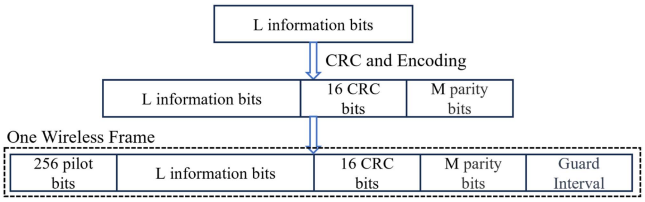

Fig. 6. Structure of the transmitted frame.

The NLOS UV communication channel exhibits significant correlation [30], where the coherent time can extend to several hundred milliseconds. Due to the requirement of precise channel state information for MCS selection, joint estimation over a long duration is adopted at the receiver. The average channel state information is adopted for selecting the transmission mode. For each M frames, the receiver provides feedback to the transmitter regarding the retransmission information. During data feedback, the receiver communicates the index of the encoding scheme and the sequence number of the erroneous data frames back to the transmitter. A feedback packet consists of synchronization sequence, HARQ retransmission information and MCS index information. To increase the reliability of the feedback link,

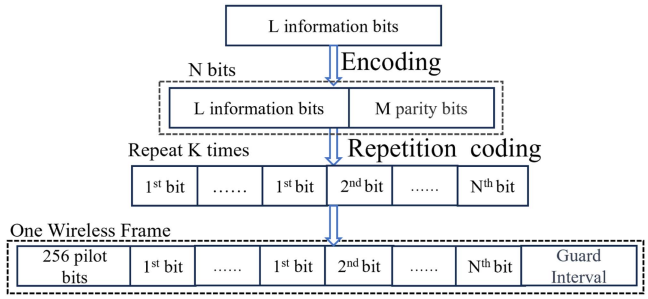

Fig. 7. Feedback link data frame structure.

LDPC codes with a four-fold spread spectrum and repetition codes are adopted. The structure of the feedback data frame is shown in Fig. 7. Since time-division is adopted for forward and feedback links, a stop-and-wait protocol is adopted.

We set the synchronization sequence length to 256 bits and the guard interval to 32 bits in the forward link and feedback link. The number of frames M transmitted consecutively each time by the transmitter is set to 20. Therefore, we need to feedback 5 bits of transmission mode information and 20 bits of retransmission information to the transmitter. Utilizing the method outlined in Section III, we construct rate-0.2 (150,30) LDPC code with a four-fold spread and conduct FER performance simulations for this LDPC code. To ensure the reliability of the feedback link, we transmit the information on the feedback link using a four-fold spread (150,30) LDPC code and a 2-fold repetition coding scheme. Therefore, the frame length of the forward transmission link is variable, and the feedback link length is 1488 bits.

V. System Design With Simulation Results

In this section, we obtain the signal strengths of NLOS links and LOS links at different transmission distances through experiments and numerical calculations, respectively. Furthermore, we constructed a simulation system by Monte Carlo algorithm and simulated the throughput of the system by the link strength of NLOS and LOS scenarios.

A. Signal Intensities for NLOS and LOS Links

In order to carry out the system throughput simulation, we need to obtain the channel parameters under the real environment. Two scenarios of non-line-of-sight link and line-of-sight link are considered. In order to investigate the channel strength of the UV non-line-of-sight link, we experimentally measured the channel strength data under the distance of 20–100 m between the transmitter and receiver when the elevation angle of the transmitter is 0 degrees and the elevation angle of the receiver is 20 degrees. Fig. 8 depicts the experimental setup of the proposed non-line-of-sight link signal strength system. At the transmitter side, we generate a 500 KHz square wave signal through an arbitrary waveform generator (AWG,33600 A Keysight) for modulation. At the receiver side, we receive the signal through a photomultiplier tube (PMT, Hamamatsu R13096). The signal received by PMT is connected to an oscilloscope (OSC, Keysight

Fig. 8. Experimental setup of the proposed NLOS link signal strength system. (a) Transmitting terminal. (b) Receiving terminal.

TABLE IV
UV NON-LINE-OF-SIGHT LINK STRENGTH MEASUREMENT PARAMETERS

Transmission power	100 mw
Transmission range	20-100 m
UV Light Wavelength	266 nm
Air-face Symbol Rate	1 Mbps
Transmitter elevation angle	0°
Receiver elevation angle	20°

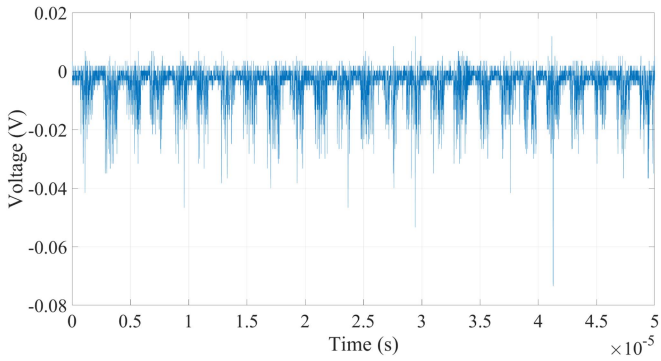

Fig. 9. The output waveform of a PMT with OOK-modulation signal.

MSOX6004 A) to sample the signal and saved for offline processing on a computer. We fix the PMT by a three-dimensional rotating platform with an adjustable elevation angle, and measure the distance between the receiver and transmitter by an ultra-wideband rangefinder (UWB) and move the receiving end of the trolley to bring the receiver and transmitter to a preset distance. The experimental parameters are shown in Table IV.

Fig. 9 illustrates the output waveform of the PMT at constant UV optical power and OOK modulation signal. Each negative pulse corresponds to one or more detectable photoelectrons, where the pulse duration is about 10 ns. The signal strength at the receiving end can be obtained by pulse counting of the received data. Fig. 10 illustrates the signal strength at different transceiver distances for an elevation angle of 20 degrees at the receiver end.

For the LOS link, the signal strength can be calculated by (2). The formula for calculating the link attenuation factor in the LOS link considering fog included is given in work [31], and

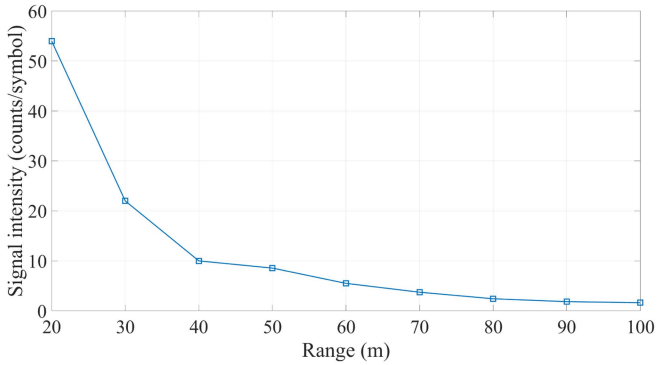

Fig. 10. The mean numbers of detected photoelectrons λ_s of the NLOS link when the symbol rate is 1 Mbps and the distance is 20–100 m.

TABLE V
UV LINE-OF-SIGHT LINK STRENGTH MEASUREMENT PARAMETERS

Transmission power	100 mw
Transmission range	200-1000 m
UV Light Wavelength	266 nm
Air-face Symbol Rate	1 Mbps
Rayleigh scattering k_s^{ray}	0.24 km^{-1}
Rayleigh absorption k_a^{ray}	0.744 km^{-1}
Receiving area S_{Rx}	1.77 cm^2

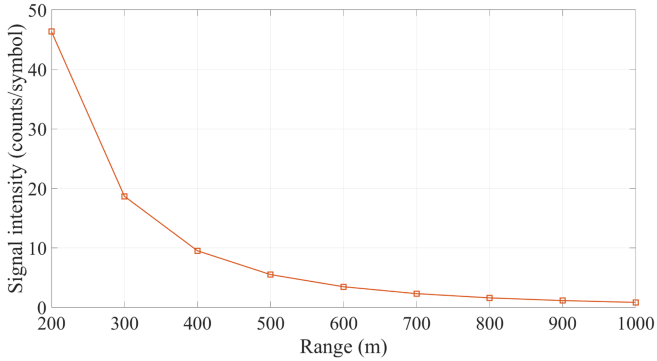

Fig. 11. The mean numbers of detected photoelectrons λ_s of the LOS link when the symbol rate is 1 Mbps and the distance is 200–1000 m.

the link attenuation is shown in (10) below when the presence of fog is not considered

$$g_t = e^{(-k_e \cdot r)} \frac{1 - r/\sqrt{r^2 + r_{Rx}^2}}{1 - cos(\phi_t/2)}, \tag{10}$$

where $k_e = k_s + k_a$, r, r_{Rx} and ϕ_t represent the sum of scattering coefficient (k_s) and absorption coefficient (k_a), the distance between the transmitter and receiver, the radius of the receiver, and the full-width beam divergence, respectively. The link parameters are shown in Table V, and the signal strength under the LOS link can be calculated as shown in Fig. 11.

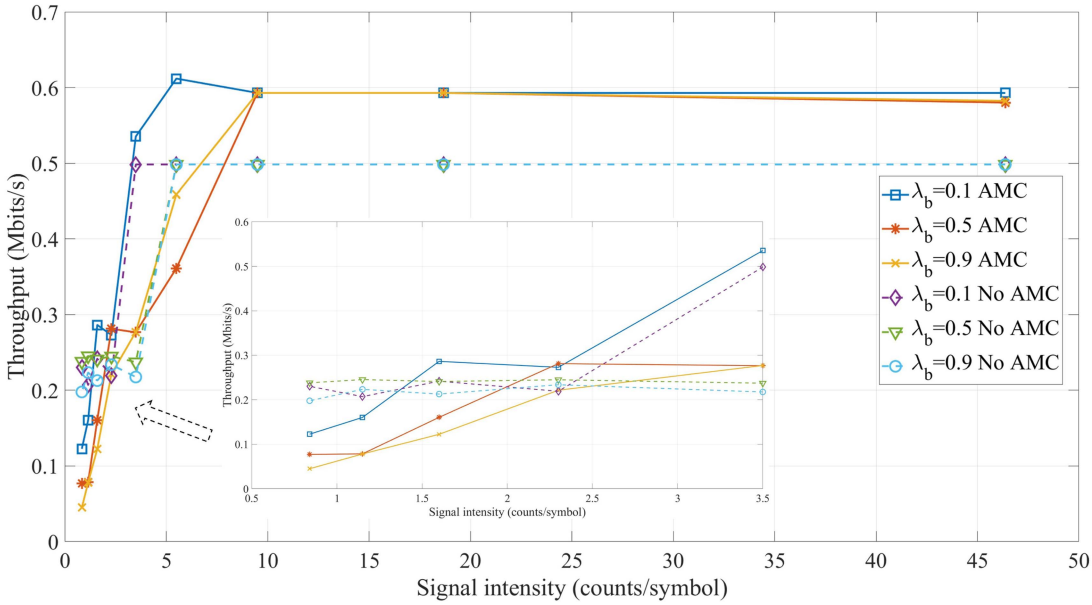

Fig. 12. The throughput for AMC and fixed-encoding-rate systems for LOS link scenarios when the symbol rate is 1 Mbps.

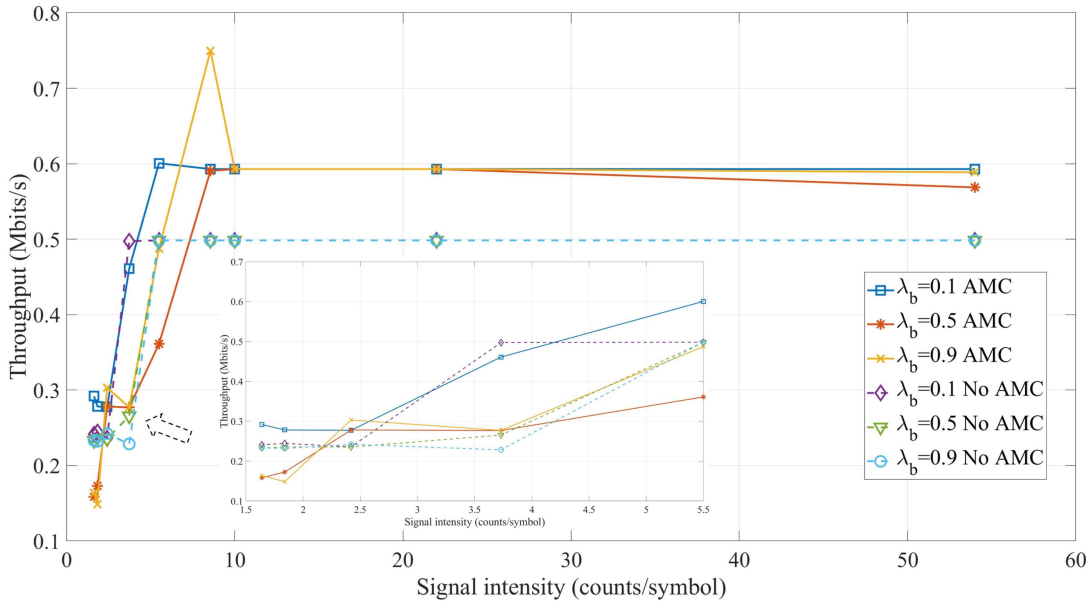

Fig. 13. The throughput for AMC and fixed-encoding-rate systems for NLOS link scenarios when the symbol rate is 1 Mbps.

B. Simulation and Analysis of Full-Link Performance in a HARQ System

In order to explore the performance of the AMC UV NLOS communication system and the system using (2176,1280) LDPC code encoding, we perform throughput simulation on these two systems. According to the system model outlined in Section II, we establish a simulation system to assess the proposed adaptive rate transmission system. This system comprises thirty selectable transmission modes with encoding switching thresholds, as depicted in Table II. In the simulation system, we set the average noise intensity sets to $\lambda_b = \{0.1, 0.5, 0.9\}$ and consider both LOS link and NLOS link scenarios, respectively. We simulated the process of end-to-end wireless UV optical communication by Monte Carlo algorithm and obtained the number of successfully received bits for the systems with AMC and only using (2176,1280) LDPC code for different signal and background intensities, respectively. Subsequently, the time required for different transmission processes is obtained based on the parameters of our designed system to get the throughput of the system.

The throughput of the AMC system and the system using (2176, 1280) LDPC codes for the LOS link and the NLOS link are shown in Figs. 12 and 13, respectively. As can be seen from

Figs. 12 and 13, the system with AMC can adjust the coding of the system according to the state information of the channel. When the channel conditions are weak, the channel coding with a longer code length and a lower code rate is adopted to maintain the reliability of the system. Thus the system throughput is not as good as that of the system with using (2176,1280) LDPC code, but the reliability of the system is stronger than it. When the channel conditions are strong, the AMC system adopts the channel coding with a higher code rate. In this way the system can improve the throughput while maintaining the reliability, and ensure that the throughput and reliability of the system are stronger than the single-coded system.

VI. Conclusion

We have designed a rate-adaptive transmission approach for UV communication and adopted HARQ to improve the system reliability, which feeds back the transmission mode index based on two-dimensional channel parameters. We have constructed 20 channel codes with different code rates and code lengths by the coding protocol based on the 5G standard, and ten spreading codes combined with low-rate LDPC codes. We have obtained the switching thresholds of the coding schemes. The channel state information for both NLOS and LOS scenarios is obtained through experiments and numerical calculations. We have also experimentally measured the end-to-end synchronization latency and constructed a simulation platform to test the throughput of the adaptive rate transmission system. Compared to the transmission using only one code, the proposed HARQ-based adaptive transmission can achieve higher throughput.

References

[1] G. A. Shaw, A. M. Siegel, and J. Model, "Extending the range and performance of non-line-of-sight ultraviolet communication links," *Proc. SPIE*, vol. 6231, pp. 93–104, 2006.

[2] Z. Xu and B. M. Sadler, "Ultraviolet communications: Potential and state-of-the-art," *IEEE Commun. Mag.*, vol. 46, no. 5, pp. 67–73, May 2008.

[3] W.-Y. Lin et al., "'10m/500 Mbps WDM visible light communication systems," *Opt. Exp.*, vol. 20, no. 9, pp. 9919–9924, 2012.

[4] C.-H. Yeh, L.-Y. Wei, and C.-W. Chow, "Using a single VCSEL source employing OFDM downstream signal and remodulated OOK upstream signal for bi-directional visible light communications," *Sci. Rep.*, vol. 7, no. 1, 2017, Art. no. 15846.

[5] W.-C. Wang, C.-W. Chow, L.-Y. Wei, Y. Liu, and C.-H. Yeh, "Long distance non-line-of-sight (NLOS) visible light signal detection based on rolling-shutter-patterning of mobile-phone camera," *Opt. Exp.*, vol. 25, no. 9, pp. 10103–10108, 2017.

[6] J.-Y. Sung, C.-W. Chow, and C.-H. Yeh, "Is blue optical filter necessary in high speed phosphor-based white light LED visible light communications?," *Opt. Exp.*, vol. 22, no. 17, pp. 20646–20651, 2014.

[7] M. R. Frey, "Information capacity of the poisson channel," *IEEE Trans. Inf. Theory*, vol. 37, no. 2, pp. 244–256, Mar. 1991.

[8] A. D. Wyner, "Capacity and error exponent for the direct detection photon channel II," *IEEE Trans. Inf. Theory*, vol. 34, no. 6, pp. 1462–1471, Nov. 1988.

[9] J. Cao, S. Hranilovic, and J. Chen, "Capacity-achieving distributions for the discrete-time Poisson channel–Part I: General properties and numerical techniques," *IEEE Trans. Commun.*, vol. 62, no. 1, pp. 194–202, Jan. 2014.

[10] A. Lapidoth and S. M. Moser, "On the capacity of the discrete-time poisson channel," *IEEE Trans. Inf. Theory*, vol. 55, no. 1, pp. 303–322, Jan. 2009.

[11] R. Yuan and M. Peng, "Single-input multiple-output scattering based optical communications using statical combining in turbulent channels," *IEEE Trans. Wireless Commun.*, vol. 23, no. 4, pp. 2560–2574, Apr. 2024.

[12] Z. Wang, R. Yuan, J. Cheng, and M. Peng, "Joint optimization of full-duplex relay placement and transmit power for multi-hop ultraviolet communications," *IEEE Internet Things J.*, vol. 11, no. 7, pp. 11960–11973, Apr. 2024.

[13] L. Qu, G. Xu, Z. Zeng, N. Zhang, and Q. Zhang, "UAV-assisted RF/FSO relay system for space-air-ground integrated network: A performance analysis," *IEEE Trans. Wireless Commun.*, vol. 21, no. 8, pp. 6211–6225, Aug. 2022.

[14] P. V. Trinh, T. C. Thang, and A. T. Pham, "Mixed mmWave RF/FSO relaying systems over generalized fading channels with pointing errors," *IEEE Photon. J.*, vol. 9, no. 1, Feb. 2017, Art. no. 5500414.

[15] H. Ding, G. Chen, A. K. Majumdar, B. M. Sadler, and Z. Xu, "Modeling of non-line-of-sight ultraviolet scattering channels for communication," *IEEE J. Sel. Areas Commun.*, vol. 27, no. 9, pp. 1535–1544, Dec. 2009.

[16] N. D. Chatzidiamantis, G. K. Karagiannidis, and M. Uysal, "Generalized maximum-likelihood sequence detection for photon-counting free space optical systems," *IEEE Trans. Commun.*, vol. 58, no. 12, pp. 3381–3385, Dec. 2010.

[17] C. Gong and Z. Xu, "LMMSE SIMO receiver for short-range non-line-of-sight scattering communication," *IEEE Trans. Wireless Commun.*, vol. 14, no. 10, pp. 5338–5349, Oct. 2015.

[18] M. A. El-Shimy and S. Hranilovic, "Spatial-diversity imaging receivers for non-line-of-sight solar-blind UV communications," *J. Lightw. Technol.*, vol. 33, no. 11, pp. 2246–2255, 2015.

[19] Q. Liu, S. Zhou, and G. B. Giannakis, "Cross-layer combining of adaptive modulation and coding with truncated ARQ over wireless links," *IEEE Trans. Wireless Commun.*, vol. 3, no. 5, pp. 1746–1755, Sep. 2004.

[20] I. B. Djordjevic, "Adaptive modulation and coding for free-space optical channels," *IEEE/OSA J. Opt. Commun. Netw.*, vol. 2, no. 5, pp. 221–229, 2010.

[21] I. B. Djordjevic and G. T. Djordjevic, "On the communication over strong atmospheric turbulence channels by adaptive modulation and coding," *Opt. Exp.*, vol. 17, no. 20, pp. 18250–18262, 2009.

[22] K. Soyjaudah and B. Rajkumarsingh, "Adaptive coding and modulation using reed solomon codes for rayleigh fading channels," in *Proc. Int. Conf. Trends Commun. Tech. Prog.*, 2001, pp. 50–53.

[23] K. Fatima, S. S. Muhammad, and E. Leitgeb, "Adaptive coded modulation for FSO links," in *Proc. 8th Int. Symp. Commun. Syst. Netw. Digit. Signal Process.*, 2012, pp. 1–4.

[24] W. Su, J. Lin, K. Chen, L. Xiao, and C. En, "Reinforcement learning-based adaptive modulation and coding for efficient underwater communications," *IEEE Access*, vol. 7, pp. 67539–67550, 2019.

[25] N. B. Halima and H. Boujemaa, "Adaptive cooperation for free space optical communications," *Telecommun. Syst.*, vol. 75, no. 1, pp. 31–41, 2020.

[26] G. Chen, F. Abou-Galala, Z. Xu, and B. M. Sadler, "Experimental evaluation of LED-based solar blind NLOS communication links," *Opt. Exp.*, vol. 16, no. 19, pp. 15059–15068, 2008.

[27] G. Wang, K. Wang, C. Gong, D. Zou, Z. Jiang, and Z. Xu, "A 1Mbps real-time NLOS UV scattering communication system with receiver diversity over 1 km," *IEEE Photon. J.*, vol. 10, no. 2, Apr. 2018, Art. no. 7903013.

[28] K. Chen, K. Niu, Z. He, and J. Lin, "Polar coded HARQ scheme with chase combining," in *Proc. IEEE Wireless Commun. Netw. Conf.*, 2014, pp. 474–479.

[29] K. Chen, K. Niu, and J. Lin, "A hybrid ARQ scheme based on polar codes," *IEEE Commun. Lett.*, vol. 17, no. 10, pp. 1996–1999, Oct. 2013.

[30] K. Wang, C. Gong, D. Zou, and Z. Xu, "Turbulence channel modeling and non-parametric estimation for optical wireless scattering communication," *J. Lightw. Technol.*, vol. 35, no. 13, pp. 2746–2756, 2017.

[31] J. Tang et al., "Ultraviolet communication with a large scattering angle via artificial agglomerate fog," *Opt. Exp.*, vol. 31, no. 14, pp. 23149–23170, 2023.